Hadronic Amplitudes

Belle II Workshop, V Tech 2025

M. V. Purohit, Univ. of S. Carolina

History of some Particle Discoveries

- The **electron**:
  - ~1700's: To explain attraction caused by rubbing, Ben Franklin thought that positive charges flowed from one material to another
  - 1838: Richard Laming hypothesized electrons as part of atoms
  - ~1891: G.J. Stoney (a.k.a. "electron Stoney") named them
  - 1897: J.J. Thomson discovered the electron by observing rays of particles streaming from the cathode to the anode.
- The **positron**:
  - Hypothesized by Dirac in 1928, discovered at Caltech ~1932
- The **proton**:
  - Rays of +ve particles emerging from anodes were observed by Eugen Goldstein in 1886, but different gases had different q/m ratios (unlike for electrons). In 1919, a decade after winning a Nobel prize, Ernest Rutherford showed that protons emerged when $\alpha + {}^{14}N \rightarrow {}^{17}O + p$.

The 1930s

- The neutron was more difficult to discover because it has no charge
- Models of the nucleus with just e and p had problems: the "Oscar Klein Paradox" of too much energy for the e (uncertainty principle), and nuclear spins. The n was discovered in 1932 by James Chadwick.
  [α + Be → neutral particles (n); n + Paraffin → p]
- Nuclear physics developed very rapidly in the 1930's: by 1938 fission had been discovered followed shortly by reactors and other applications.
- 1935: Fermi *et al*. Showed that n are very effective at disintegrating nuclei.
  Bethe explained this beautifully in a 1935 paper.

"Theory of Disintegration of Nuclei by Neutrons", by H.A. Bethe, Phys. Rev. 47.747 (1935)

The large probability of nuclear disintegration by slow neutrons as well as the large cross section for the elastic scattering of slow neutrons can be explained without any new assumption. Interaction between neutron and nucleus is assumed to be only present when the neutron is inside the nucleus or very near its boundary. The rate of change of the potential energy of the neutron at the boundary of the nucleus is important for the quantitative, but not for the qualitative results; in agreement with other data, it has been assumed that the potential drops to $1/e$ in a distance $1.5.10^{-13}$ cm (range of the forces between neutron and nucleus).

The large disintegration cross sections are due to two factors. The first is elementary: the cross section is inversely proportional to the neutron velocity, because a slow neutron stays longer in the nucleus. The second factor is $1/\sin^2 \varphi_0$, where φ_0 is the phase of the neutron wave function at the nuclear boundary. This resonance factor explains the large differences between the cross sections of different elements. φ_0 cannot be predicted theoretically, but reasonable assumptions lead to agreement with experiment. The resonance factor occurs in all phenomena with slow neutrons; therefore large capture cross sections should always be accompanied by large elastic scattering. The explanation of the large neutron cross sections on the basis of ordinary wave mechanics makes one confident in the applicability of orthodox quantum theory in nuclear phenomena.

Belle II

Nuclear Potential + Centrifugal Barrier

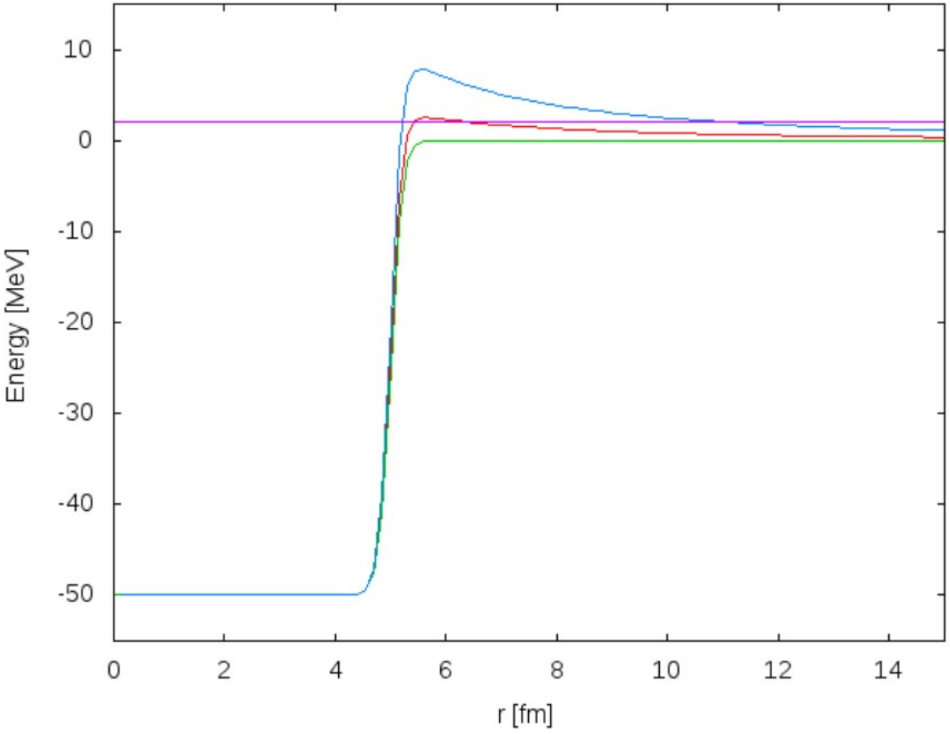

- Potential for nuclear interactions assumed to have -50 MeV depth and radius of 5 fm. Graphs are:
  - green for l=0 $\hbar$
  - red for l=1 $\hbar$
  - blue for l=2 $\hbar$
  - purple for E = 2 MeV.

[From https://web-docs.gsi.de/~wolle/TELEKOLLEG/KERN/LECTURE/Fraser/L21.pdf]

Scattering of incoming particles: what we learn from Bethe's paper

- We commonly assume that the incoming particles come along the z-axis and collide with the target at the origin.

- The incoming wave is ~ exp(ikz), which can be resolved into incoming spherical waves.

- At typically low energies, only S-waves ($\ell = 0$) contribute because higher ℓ-values correspond to larger distances; alternatively the "centrifugal barrier" is higher.

$\sigma_{\text{fiss.}}$ vs. neutron energy at low energies

Resonances

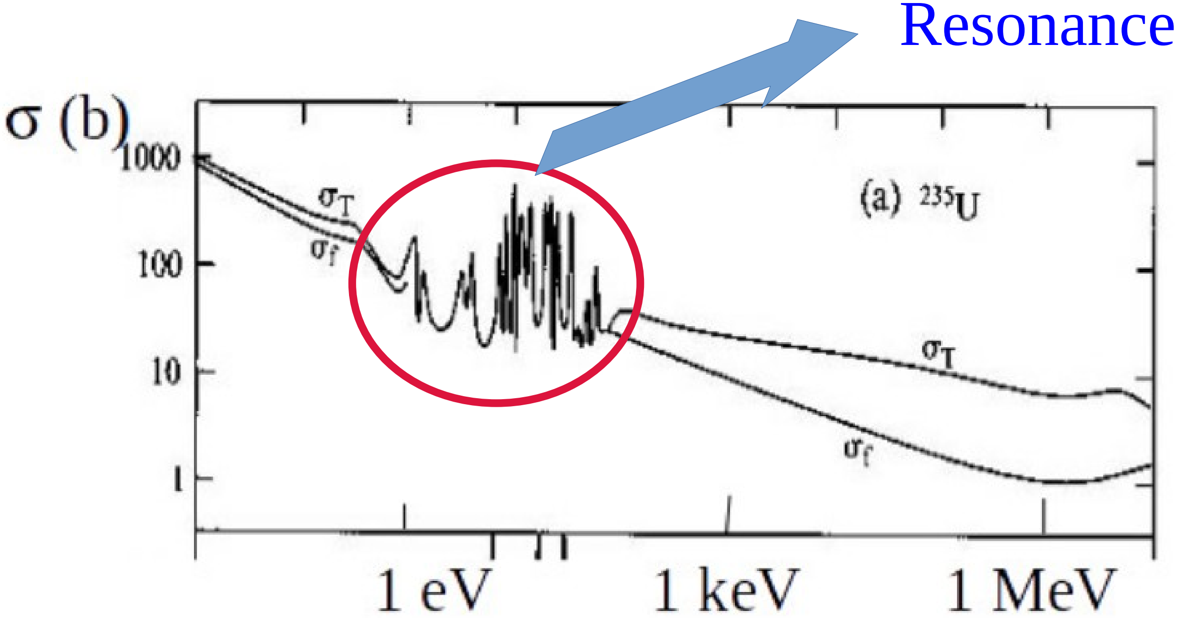

From online lecture notes of

Prof. Tina Potter

UNIVERSITY OF CAMBRIDGE

Blatt & Weisskopf (1952)

The wave function u_l just inside the nuclear boundary $(r<R)$ can no longer be represented by (4.6), which symbolizes an ingoing wave only. It now must include also a term representing a wave returning toward the outside. This is indicated by

$$u_l \sim \exp(-iKr_\alpha) + \mathfrak{b}\exp(+iKr_\alpha) \qquad (\text{for } r < R) \tag{7.1}$$

where $\mathfrak{b}$ is the (complex) amplitude of the returning wave and depends on the properties of the compound nucleus. At high incident energies we expect $\mathfrak{b}$ to be close to zero. In absolute value, $\mathfrak{b}$ is never larger than unity, since no more particles can approach $r_\alpha = R$ from the interior in channel α than have originally penetrated into the inside region.

It must be emphasized again that (7.1) is not an exact representation of the wave function u_l inside the nucleus. For $r<R$, the wave function describing the motion of the incident particle depends on the variables of all other nucleons involved; it is no longer described by a one-particle function $u_l(r_\alpha)$. Relation (7.1) is a very approximate expression which is used to describe only the main features of the dependence of the actual wave function on r_α near the nuclear surface. It expresses the fact that the incident particle possesses an average wave number K, and that it has a finite chance to return into the entrance channel. We are using (7.1) only to determine the logarith-

Caveat:

Potential is approximate

Belle

SC HEP

Blatt & Weisskopf, continued

Let us now consider the opposite extreme where the energy of the incident particle is so low that *no other channel but the entrance channel is open*, so that the compound system can decay *only* by re-emitting the incident particle with the same energy with which it entered. An example of this is a reaction in which the incident beam consists of neutrons of an energy ϵ, smaller than the lowest excitation energy of the target nucleus, and smaller than the threshold of any nuclear reaction. (In general, an energy $\epsilon < 100$ kev will fulfill this condition if we neglect the possibility of radiative capture and fission.) Then the neutron must leave the compound nucleus again with an energy ϵ.

The wave function inside the surface can then be approximated by

$$u_l \sim \exp(-iKr_\alpha) + \exp[i(Kr_\alpha + 2\zeta)] \tag{7.2}$$

in which the incoming and outgoing waves are equally strong ($|b| = 1$),

Blatt & Weisskopf, continued

the outgoing wave having a phase shift 2ζ (ζ=real). The boundary condition at $r_\alpha = R$ on the wave function is now

Logarithmic Derivative

$$f_l = R\left(\frac{du_l/dr}{u_l}\right)_{r=R} = -KR\tan\left[KR + \zeta(\epsilon)\right] \tag{7.3}$$

(7.3) is quite different from (4.7). The phase $\zeta(\epsilon)$ with which the wave returns depends quite sensitively on the complicated interactions which the particle undergoes within the nucleus before it re-emerges near the surface, and is therefore a function of the energy of the entering particle. The cross sections, which follow from (7.3), will be calculated in Section 8. In this section we restrict ourselves to qualitative reasoning, and an attempt will be made to explain or to make plausible the most important qualitative features of the resonance phenomena. The quantitative calculations and the more rigorous derivations are found in the succeeding sections, and in Chapter X.

The re-emergence of the particle gives rise to the *occurrence of resonances* in the compound system. This can be seen qualitatively in the following way:[1] Expression (7.2) shows that the wave function just inside the nuclear surface can be written in the form

$$u \sim C\cos\left[Kr + \zeta(\epsilon)\right] \qquad (\text{for } r < R) \tag{7.4}$$

where C is a constant. This function must be joined smoothly to

Blatt & Weisskopf, continued

incident particle in general penetrates very little into the nucleus. There is, however, a series of energy values ϵ_s, the "resonance" energies, for which $\zeta(\epsilon_s)$ has the right value, so that the tangent of u_l is horizontal at $r=R$. In the neighborhood of these energies the wave penetrates strongly into the nucleus. Hence the particle can enter the nucleus and form a "compound state" only if the energy ϵ is equal or nearly equal to a "resonance" energy ϵ_s.

More conclusions can be drawn from our picture regarding the scattering cross section. The smallness of C/A for energies off resonance implies also that the outside wave assumes a very small

Belle II

USC HEP
University of South Carolina
High Energy Physics Group

Blatt & Weisskopf, continued

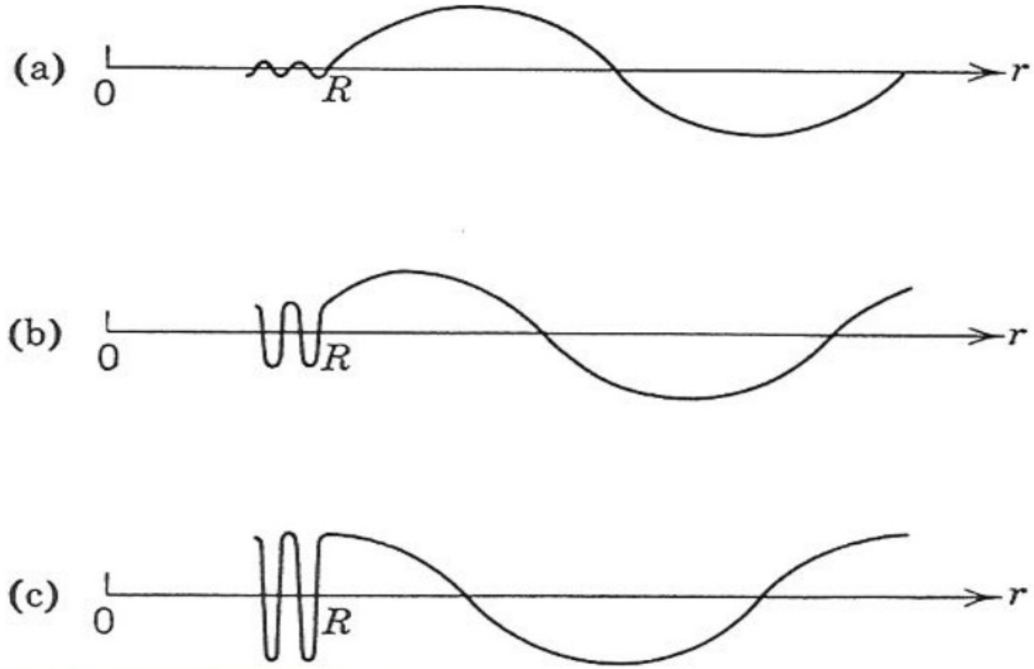

FIG. 7.1. Schematic representation of neutron wave functions at the nuclear surface. The wave functions are indicated as functions of the distance r from the center of the nucleus. $r = R$ is the nuclear radius. Case (a) corresponds to a neutron energy between resonances, case (b) is near resonance, case (c) is in resonance.

value at $r = R$. It almost could be written in the form $A \sin k(r - R)$, which reaches zero at $r = R$. This would be just the solution for the scattering at an impenetrable sphere of radius R, which would force the wave function to vanish at $r = R$. Thus we conclude that the scattering away from resonance ought to be almost identical with that of an impenetrable sphere of radius R.[1]

Breit & Wigner, 1936

In their 1936 paper, G. Breit & E. Wigner, Phys. Rev. 49, 519 state:

$$S=2L+1 \qquad (13)$$

in these special circumstances. For s terms $S=1$. The total cross section

$$\sigma=\sigma_c+\sigma_s,$$

where σ_s is the cross section due to scattering and σ_c is the cross section due to capture. We have

$$\sigma_c=\frac{\Lambda^2}{\pi}S\frac{\Gamma_s\Gamma_r}{(\nu-\nu_0)^2+\Gamma^2}; \quad \sigma_s=\frac{\Lambda^2}{\pi}S\frac{\Gamma_s{}^2}{(\nu-\nu_0)^2+\Gamma^2}. \qquad (14)$$

The above value of σ_s corresponds to the value $\Sigma|a_s|^2$ and does not take into account the fact that there is scattering in the absence of the quasi-stationary level. If this is strong one must correct σ_s for interference of the states s with the spherical wave present in s_0. In the applications made below the scattering effect due to either cause will be small and the correction need not be considered. According to (14) the extra scattering can be expected to be of the order Γ_s/Γ_r times the capture and is quite small for small Γ_s.

Caveat:

The states "s" of the free neutron are assumed not to interfere with scattered states; if so, interference must be accounted for.

Belle II

USC HEP
University of South Carolina
High Energy Physics Group

General description of Decays

- There are 3 degrees of freedom (momenta) for each final state particle, and 4 energy-momentum constraints. Thus, for an n-body decay we expect (3n – 4) degrees of freedom. Calculations are usually done in the rest frame of the decaying particle.
- In a 2-body decay, $0 \rightarrow 1+2$, the final state has 2 degrees of freedom. The energies and momenta of 1 and 2 are fixed, while the azimuthal and polar angles of the back-to-back decay line are not.
- In a 3-body decay, there should be 5 degrees of freedom. If the decaying particle is spinless, e.g., a B-meson, there is no dependence on the direction of one particle, eliminating two degrees of freedom. The azimuthal angle of the other two around this direction can also be eliminated, leaving us with two degrees of freedom: E_2 and E_3, or some other variation thereof.

From the PDG: Decays

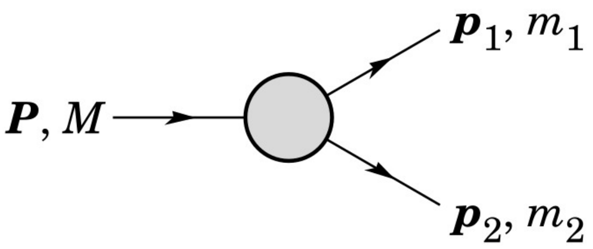

49.4 Particle decays

The partial decay rate of a particle of mass M into n bodies in its rest frame is given in terms of the Lorentz-invariant matrix element $\mathscr{M}$ by

$$d\Gamma = \frac{(2\pi)^4}{2M} \, |\mathscr{M}|^2 \, d\Phi_n \, (P;\, p_1, \ldots, p_n), \tag{49.11}$$

where $d\Phi_n$ is an element of n-body phase space given by

$$d\Phi_n(P;\, p_1, \ldots, p_n) = \delta^4 \left(P - \sum_{i=1}^{n} p_i\right) \prod_{i=1}^{n} \frac{d^3 p_i}{(2\pi)^3 2E_i} \; . \tag{49.12}$$

This phase space is reduced by combinatoric factors whenever there are identical particles in the final state. The phase space can be generated recursively, viz.

$$\begin{aligned} d\Phi_n(P;\, p_1, \ldots, p_n) &= d\Phi_j(q;\, p_1, \ldots, p_j) \\ &\times \; d\Phi_{n-j+1} \, (P;\, q, p_{j+1}, \ldots, p_n)(2\pi)^3 dq^2 \; , \end{aligned} \tag{49.13}$$

where $q^2 = \left(\sum_{i=1}^{j} E_i\right)^2 - \left|\sum_{i=1}^{j} \boldsymbol{p}_i\right|^2$. This form is particularly useful in the case where a particle decays into another particle that subsequently decays.

From the PDG: Scattering

49.3 Lorentz-invariant amplitudes

The matrix elements for a scattering or decay process are written in terms of an invariant amplitude $-i\mathscr{M}$. As an example, the S-matrix for $2 \to 2$ scattering is related to $\mathscr{M}$ by

$$\langle p_1' p_2' \, |S - 1| \, p_1 p_2 \rangle = i(2\pi)^4 \, \delta^4(p_1 + p_2 - p_1' - p_2') \mathscr{M}(p_1, \, p_2; \, p_1', \, p_2') \; . \tag{49.8}$$

The state normalization is such that

$$\langle p' | p \rangle = (2\pi)^3 \, 2E_p \, \delta^3(\boldsymbol{p}' - \boldsymbol{p}) \; , \tag{49.9}$$

with $E_p = \sqrt{\boldsymbol{p}^2 + m^2}$.

For a $2 \to 2$ scattering process producing unstable particles $1'$ and $2'$ decaying via $1' \to 3'4'$ and $2' \to 5'6'$ the matrix element for the complete process can be written in the narrow width approximation as:

vs BW

$$\mathscr{M}(12 \to 3'4'5'6') = \sum_{h_{1'}, h_{2'}} \frac{\mathscr{M}(12 \to 1'2')\mathscr{M}(1' \to 3'4')\mathscr{M}(2' \to 5'6')}{(m_{3'4'}^2 - m_{1'}^2 + i m_{1'}\Gamma_{1'})(m_{5'6'}^2 - m_{2'}^2 + i m_{2'}\Gamma_{2'})} \tag{49.10}$$

Here, m_{ij} is the invariant mass of particles i and j, m_k and Γ_k are the mass and total width of particle k, and the sum runs over the helicities of the intermediate particles. This enables the cross section for such a process to be written as the product of the cross section for the initial $2 \to 2$ scattering process with the branching ratios (relative partial decay rates) of the subsequent decays. A more sophisticated treatment, beyond the narrow width approximation, can be found in the review on "Resonances".

From the PDG: Resonances

Resonance phenomena are very rich: while typical hadronic widths are of the order of 100 MeV (*e.g.*, for the meson resonances $\rho(770)$ or $\psi(4040)$ or the baryon resonance $\Delta(1232)$) corresponding to a lifetime of 10^{-23} s, the widths can also be as small as a few MeV (*e.g.* of $\phi(1020)$ or J/ψ) or as large as several hundred MeV (*e.g.* of the meson resonances $f_0(500)$ or $D_1(2430)$ or the baryon resonance $N(2190)$).

Typically, a resonance appears as a peak in the total cross section. If the structure is narrow and if there are no relevant thresholds or other resonances nearby, the resonance properties may be extracted employing a Breit–Wigner parameterization, if necessary improved by using an energy-dependent width (*cf.* Sec. 50.3.1 of this review). However, in general, unitarity and analyticity call for the use of more refined tools as outlined here as well as in recent review articles [1, 2]. When there are overlapping resonances with the same quantum numbers, the resonance terms should not simply be added but combined in a non-trivial way either in a $\mathcal{K}$-matrix approach (*cf.* Sec. 50.3.2 of this review) or using other advanced methods (*cf.* Sec. 50.3.5 of this review). Additional constraints from the $\mathcal{S}$-matrix allow one to build more reliable amplitudes and, in turn, to reduce the systematic uncertainties of the resonance parameters: pole locations and residues. In addition, for broad resonances there is no direct relation between pole location and the total width/lifetime — then, the pole residues need to be used in order to quantify the decay properties.

For simplicity, throughout this review the formulas are given for resonances in a system of distinguishable, scalar particles. The additional complications that appear in the presence of spins can be controlled in the helicity framework developed by Jacob and Wick [3], or in a non-covariant [4] or covariant [5] tensor-operator formalisms. Within these approaches, sequential (cascade) decays are commonly treated as a coherent sum of two-body interactions. Most of the expressions below are given for two-body kinematics.

PDG: 3-body Decays

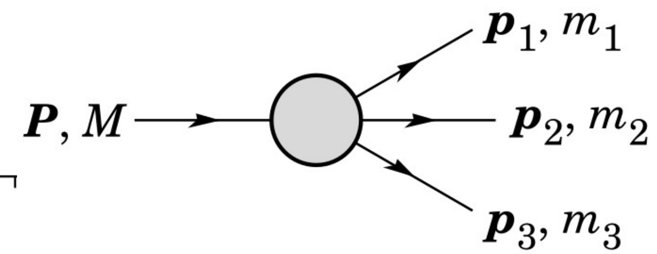

$$d\Gamma = \frac{1}{(2\pi)^3}\frac{1}{8M}\overline{|\mathscr{M}|^2}\,dE_1\,dE_3$$
$$= \frac{1}{(2\pi)^3}\frac{1}{32M^3}\overline{|\mathscr{M}|^2}\,dm_{12}^2\,dm_{23}^2\,.$$

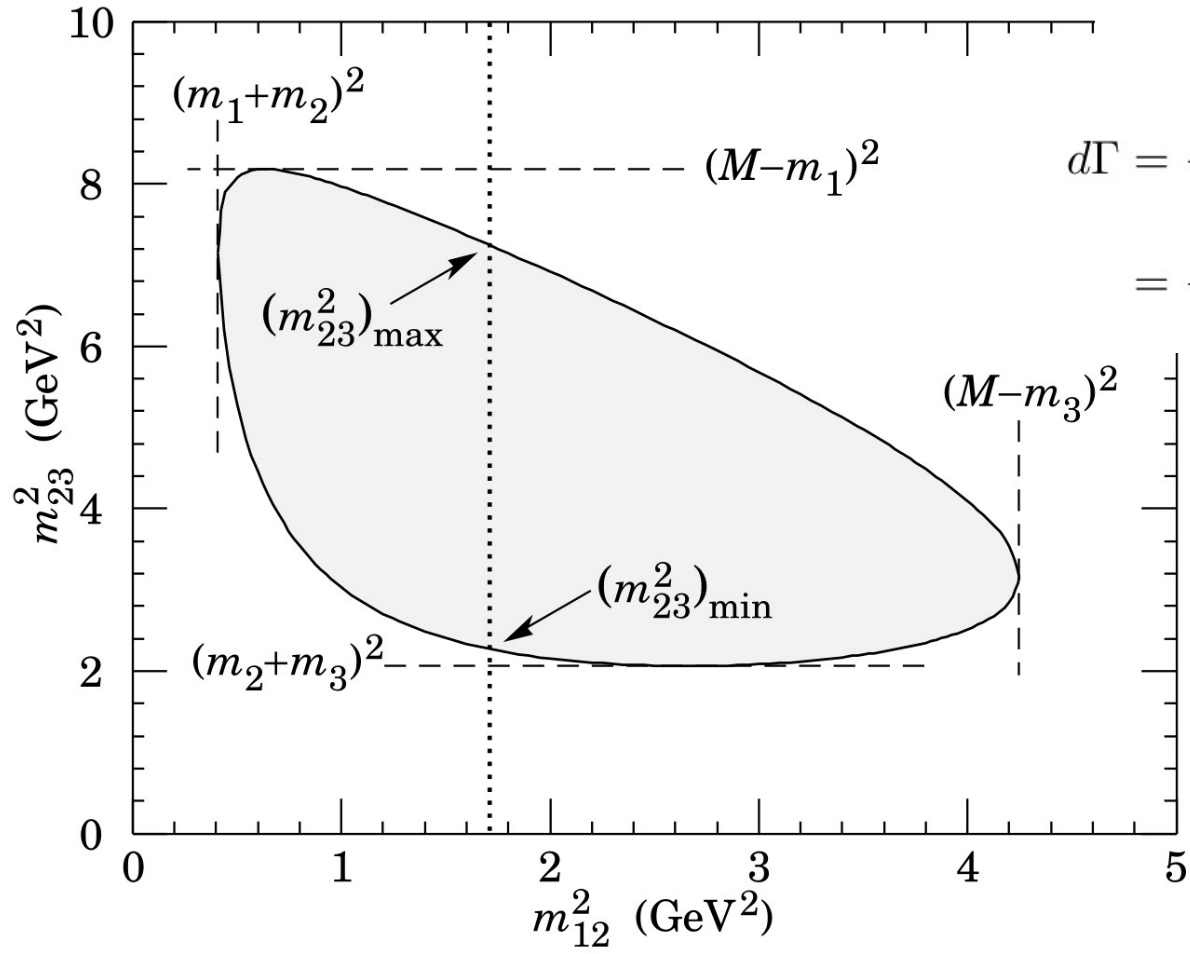

Figure 49.3: Dalitz plot for a three-body final state. In this example, the state is $\pi^+\overline{K}^0p$ at 3 GeV. Four-momentum conservation restricts events to the shaded region.

Dalitz Example 1

Recent charm results from Belle Longke Li

https://arxiv.org/pdf/2102.03703

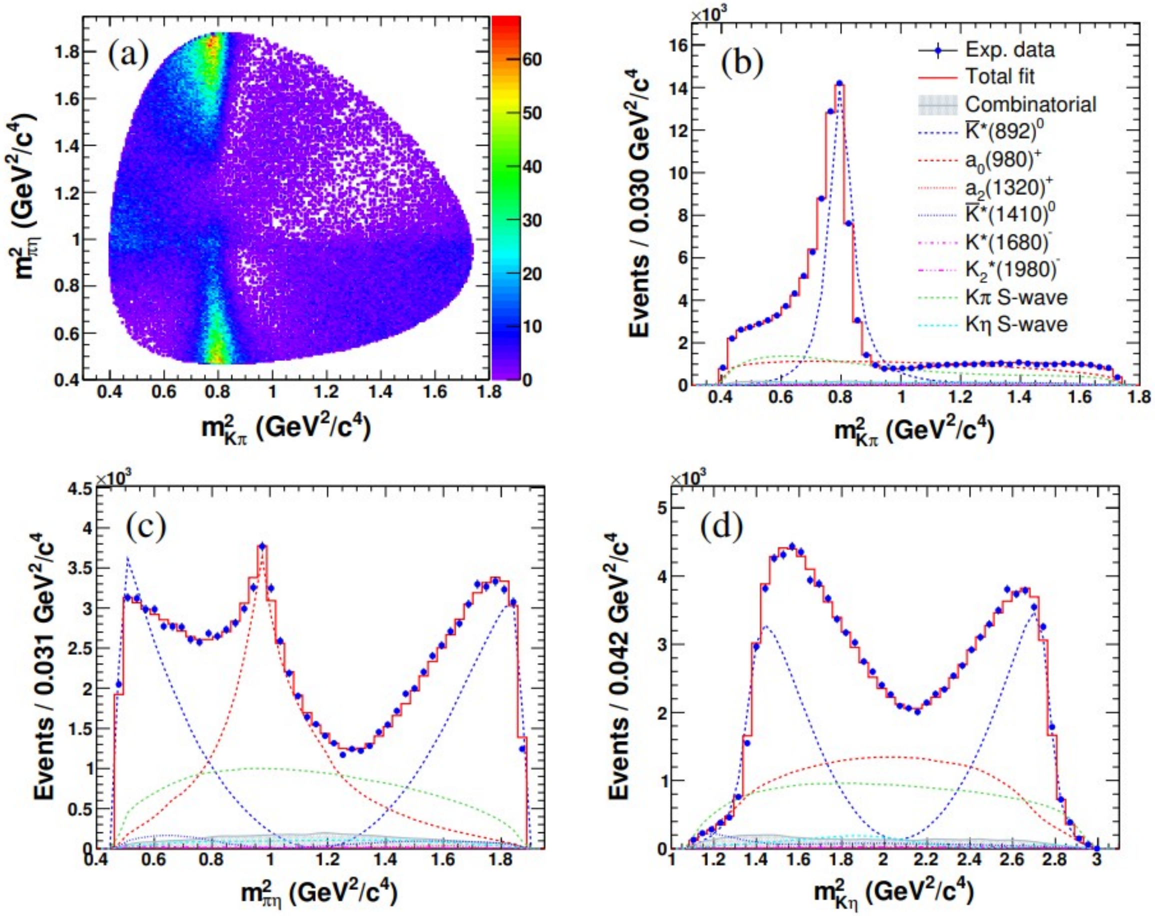

Figure 2: The Dalitz plot of $D^0 \to K^-\pi^+\eta$ in (a) M-Q signal region $1.85\ \mathrm{GeV}/c^2 < M < 1.88\ \mathrm{GeV}/c^2$ and $5.35\ \mathrm{MeV}/c^2 < Q < 6.35\ \mathrm{MeV}/c^2$, and projections on (b) $m^2_{K\pi}$, (c) $m^2_{\pi\eta}$ and (d) $m^2_{K\eta}$. In projections the fitted contributions of individual components are shown, along with contribution of combinatorial background (grey-filled) from sideband region.

Belle II

HEP

Dalitz Example 2

https://arxiv.org/pdf/2102.03703

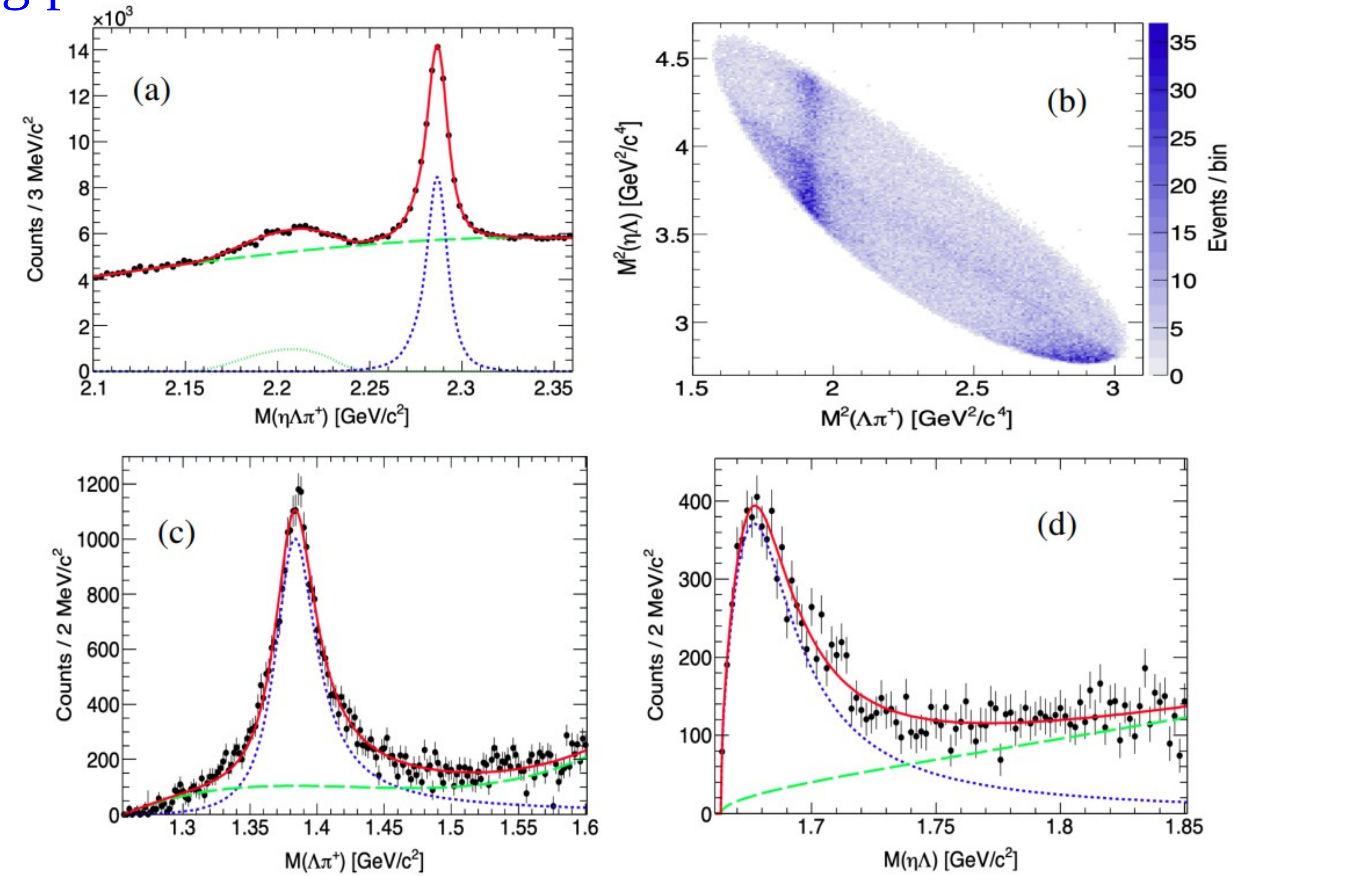

Figure 3: Top figures are (a) the invariant mass of $\eta\Lambda\pi^+$ and (b) its Dalitz plot in signal region. Bottom figures are fits to the Λ_c^+ yield in the (c) $M(\eta\Lambda)$ and (d) $M(\Lambda\pi^+)$ spectra, where the curves indicate the total fit result (solid red), the signal modeled with a relativistic Breit-Wigner function (dashed blue), and the background (long-dashed green).

Some results from Scattering Theory (see PDG note on "Resonances")

- The reaction amplitude can be expressed as a function of two variables, $\mathcal{M}(s,t)$.
- The Optical Theorem: $\mathrm{Im}\,\mathcal{M}_{aa}(s,0) = 2q_a\sqrt{s}\,\sigma_{\mathrm{tot}}(a \to \text{anything})$
- Partial wave expansion of the scattering amplitude (scalars; a→b):

$$\mathcal{M}_{ba}(s,t) = \sum_{j=0}^{\infty}(2j+1)\mathcal{M}^{j}_{ba}(s)P_j(\cos(\theta))$$

Upon normalizing the scattering amplitude by phase space factors:

$$f_{ba}(s) = \sqrt{\rho_b}\,\mathcal{M}_{ba}(s)\,\sqrt{\rho_a}\,. \qquad (50.12)$$

The unitarity condition for f_{ba} follows from Eq. (50.10):

$$\mathrm{Im}\,f_{ba}(s) = \sum_c f^*_{cb}(s)f_{ca}(s)\,. \qquad (50.13)$$

It leads us to deduce that the inverse of the imaginary part of f_{ba} is equal to $-\delta_{ba}$. Moreover, $\mathcal{S} = \mathbb{I} + 2if$ is a unitary matrix. Hence, the diagonal elements of f can be parameterized as

$$f_{bb} = (\eta_b \exp(2i\delta_b) - 1)/2i\;, \qquad (50.14)$$

Some results from Scattering Theory, continued

where δ_b denotes the phase shift for the scattering from channel b to channel b and η_b is the elasticity parameter, also known as inelasticity. Building upon Eq. (50.13), we can further deduce that,

$$\operatorname{Im} f_{bb}(s) = (1 - \eta_b \cos(2\delta_b))/2 = \sum_c |f_{cb}(s)|^2 . \tag{50.15}$$

Using Eq. (50.14) for the last term in the sum, we obtain a relation highlighting the meaning of the inelasticity,

$$\frac{1}{4}(1 - \eta_b^2) = \sum_{c \neq b} |f_{cb}(s)|^2 . \tag{50.16}$$

It is important to note that the parameter η_b is confined within the range $[0, 1]$, where the case, $\eta_b = 1$ is referred to as a purely elastic scattering. Thus, the function $\eta_b(s)$ is a direct measure of the contribution of the inelastic channels on the scattering amplitude in a given channel.

The evolution of the partial-wave amplitude f_{bb} with energy can be displayed as a trajectory in the Argand plot, as shown in Fig. 50.5. In case of a two-channel problem, $\eta_1 = \eta_2 = \eta$, and the off-diagonal element is $f_{12} = \sqrt{1 - \eta^2}/2 \exp(i(\delta_1 + \delta_2))$. The unitarity condition Eq. (50.14) sets the limit to the squared amplitude f_{bb}:

$$|f_{bb}|^2 = \frac{1}{4}(\eta_b^2 - 2\eta_b \cos(2\delta_b) + 1) \leq \frac{1}{4}(\eta_b + 1)^2 , \tag{50.17}$$

Some results from Scattering Theory, continued

where the maximum value is reached for $\delta_b = \pi/2$. For the absolute square of the partial-wave-projected scattering amplitude the unitarity bound thus reads:

$$|\mathcal{M}_{bb}| \;\leq\; \frac{1}{2\rho_b}(\eta_b + 1) \;\leq\; \frac{8\pi}{q_b}\sqrt{s}\,, \tag{50.18}$$

where the second inequality comes from $\eta_b \leq 1$. For energies much larger than the masses of the scattering particles the upper bound for $|\mathcal{M}_{bb}|$ tends to 16π for large s.

The partial-wave projected production amplitude $\mathcal{A}(s)$ (note that the label j has been omitted for consistency) is also constrained by unitarity. As derived from Eq. (50.8):

$$\mathrm{Im}\,\mathcal{A}_a = \sum_b \mathcal{M}^*_{ba}\,\rho_b\,\mathcal{A}_b\ , \tag{50.19}$$

where the summation encompasses all open channels. In the realm of elastic scattering, solely one channel, denoted by a, contributes to the sum. Consequently, the phase of $\mathcal{A}_a$ must align with the phase of $\mathcal{M}_{aa}$, given that the left-hand side of Eq. (50.19) represents a real value. This principle is recognized as the *Watson theorem* [57]. To illustrate, consider the phase of the pion vector form factor: it agrees to that of $\pi\pi$ scattering in the vector isovector channel (aside from effects of the isospin-violating $\rho-\omega$ mixing) up to about 1 GeV, where inelastic contributions start gaining significance.

50.3.1 *The Breit–Wigner parameterization*

The relativistic Breit–Wigner parameterization represents a dressed propagator for an isolated resonance. The production amplitude for a resonance observed in a channel a, is given by

$$\boxed{\mathcal{A}_a(s) = \frac{\mathcal{N}_a(s)}{M_{\mathrm{BW}}^2 - s - iM_{\mathrm{BW}}\Gamma(s)}} \tag{50.30}$$

where M_{BW} represents the Breit–Wigner mass, and $\Gamma_{\mathrm{BW}} = \Gamma(M_{\mathrm{BW}}^2)$ denotes the Breit–Wigner width. The function $\Gamma(s)$ is defined by the channels to which the resonance can decay. The numerator function $\mathcal{N}_a(s)$ is tailored to the production process, encompassing kinematic factors and couplings pertinent to both the production and decay processes.

$$\mathcal{N}_a(s) = \alpha\, g_a\, n_a(s) \tag{50.31}$$

$$\Gamma(s) = \frac{1}{M_{\mathrm{BW}}} \sum_b g_b^2 \rho_b(s) n_b^2(s)\ , \tag{50.32}$$

Here the index $b = 1, 2, \ldots$ runs over all decay channels of the resonance. The coupling constants are represented by g_b, and ρ_b is the phase-space factor as defined in Eq. (50.11). The expression for $n_a(s)$ is:

$$\boxed{n_a = (q_a/q_0)^{l_a} F_{l_a}(q_a/q_0)} \tag{50.33}$$

where l_a indicates the orbital angular momentum in channel a, $q_a(s)$ is the break-up momentum as defined in Eq. (50.7), and q_0 is a suitably selected momentum scale. The term $(q_a)^{l_a}$ ensures the amplitude's appropriate threshold behavior. The rapid growth of this factor for angular momenta $l_a > 0$ is offset at specific s values by a phenomenological form factor, represented here by $F_{l_a}(q_a, q_0)$ — the presence of these suppression factors is also a requirement from positivity which demands that the dressed propagator, the denominator of Eq. (50.30) and similar equations below, is not allowed to drop faster than $1/s$ [27]. The Blatt-Weisskopf form factors are frequently employed in the literature [70–72] to model F_j:

$$F_0^2(z) = 1\,, \tag{50.34}$$
$$F_1^2(z) = 1/(1+z^2)\,,$$
$$F_2^2(z) = 1/(9+3z^2+z^4)\,,$$

where $z = q/q_0$, the scale parameter $1/q_0$ typically falls within the range of $1\,\mathrm{GeV}^{-1}$ to $5\,\mathrm{GeV}^{-1}$.

Partial wave decomposition

50.1.3 *Partial-wave decomposition*

It is often convenient to expand a two-body scattering amplitude of a two-body subsystem of a production amplitude in partial waves. Since resonances have a well-defined spin, they appear only in a specific partial wave of the reaction amplitude. For scalar particles, the expansion reads:

$$\boxed{\mathcal{M}_{ba}(s,t) = \sum^{\infty}(2j+1)\mathcal{M}^{j}_{ba}(s)P_j(\cos(\theta))} \tag{50.9}$$

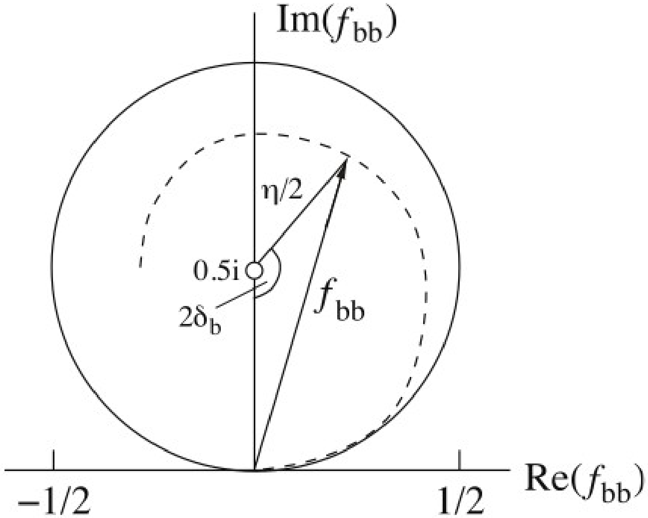

Figure 50.5: Argand plot showing a trajectory of the diagonal element of a partial-wave amplitude, f_{bb}, as a function of energy in the complex plane. As the energy increases the amplitude follows the line counter clockwise. The amplitude leaves the unitary circle (solid line) as soon as inelasticity sets in, $\eta < 1$ (dashed line).

More caveats (PDG)

Equation (50.32) incorporates a threshold for each of the coupled channels. The expression is straightforward to use in the physical region above all the thresholds. Its evaluation elsewhere requires a careful analytic continuation. As outlined in Refs. [73, 74], the choice

the physical region of the lighter channel computed with Eq. (50.36). When a resonance's coupling to the channel with a higher threshold is notably strong, the parameterization displays scaling invariance. This implies that it is not possible to extract individual partial decay widths; only their ratios can be determined [75].

The Breit–Wigner parameterization is an accurate representation of resonance phenomena strictly in the $\Gamma/\Delta \to 0$ limit, where Γ is the resonance width and Δ is the distance to the closest unaccounted singularity, be it a pole of a higher resonance or a kinematic threshold related to a coupled channel. However, the situation is often more complex due to multiple singularities in the complex plane around the resonance with different importance. For instance, in P-wave $\pi\pi$ scattering, the Breit–Wigner parameterization aptly describes the ρ-meson resonance over an

applicability. If there is more than one resonance in one partial wave that significantly couples to the same channel, it is generally inappropriate to employ a sum of Breit–Wigner functions. Such an approach often results in a breach of unitarity constraints, potentially introducing an indeterminate bias to the inferred resonance properties from the reaction amplitude. For overlapping resonances in the same partial wave, more sophisticated methods, such as the $\mathcal{K}$-matrix approach detailed in the subsequent section, are recommended.

Enforcing Unitarity

50.3.2 $\mathcal{K}$-*matrix approach*

The $\mathcal{K}$-*matrix* method offers a comprehensive framework for modelling coupled-channel amplitudes [78]. This method ensures two-particle unitarity. However, it traditionally omits the left-hand cuts. The scattering amplitude $\mathcal{M}_{ba}(s)$ can be derived from the equation:

$$n_b\,\mathcal{M}^{-1}_{ba}\,n_a = \mathcal{K}^{-1}_{ba} - i\delta_{ba}\rho_a n_a^2\,. \tag{50.37}$$

Here, $\mathcal{K}_{ba}$ represents a real function and is subject to modeling. The factor n_a is elaborated upon in Eq. (50.33). Since there is no unique recipe to build $\mathcal{K}$, it is essential to explore various parameterizations to gauge the theoretical systematic uncertainty. A commonly adopted choice for the $\mathcal{K}$-matrix is given by:

$$\boxed{\mathcal{K}_{ba}(s) = \sum_{\mathrm{R}} \frac{g_b^{\mathrm{R}} g_a^{\mathrm{R}}}{m_{\mathrm{R}}^2 - s} + b_{ba}\,,} \tag{50.38}$$

where m_{R} is referred to as the bare mass of the resonance R (not to be confused with the physical mass), and the g_a^{R} represents the bare couplings of the resonance R to the channel a (not to be confused with the residues). The b_{ba} is a matrix that parameterizes the non-pole components of the $\mathcal{K}$-matrix. Provided all parameters in Eq. (50.38) are real, the amplitude $\mathcal{M}_{ba}(s)$ remains unitary. From Eq. (50.37), the scattering amplitude $\mathcal{M}$ can be directly computed using its matrix form:

$$\boxed{\mathcal{M} = n[1 - \mathcal{K}\,i\rho\,n^2]^{-1}\mathcal{K}\,n} \tag{50.39}$$

We skip over Q-vectors, P-vectors, …, lattice gauge calculations, ...

Final Note from the PDG review

There has been considerable interest in the $3 \to 3$ scattering recently, particularly in light of new data on three-hadron interaction [127] and advancements in lattice calculations [128]. One finds that the methodologies devised for accounting for one-pion exchange bear a resemblance to the two-potential decomposition. For details see Ref. [129], also Eq. (93) in Ref. [130].

BaBar: Dalitz Plot Analysis of $D_s^+ \to \pi^+\pi^-\pi^+$

~13,000 events

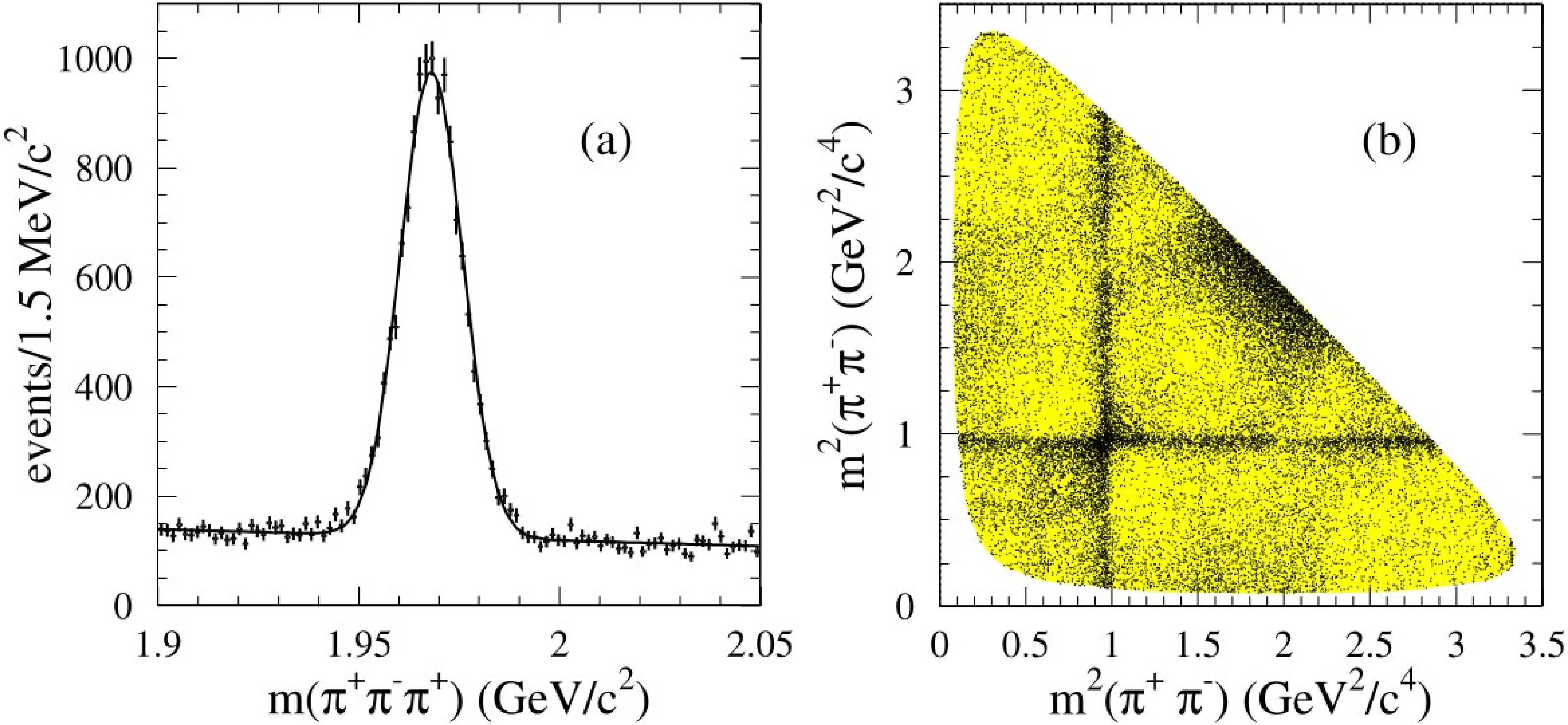

BaBar: Dalitz Plot Analysis of $D_s^+ \to \pi^+\pi^-\pi^+$

The $\pi^+\pi^-$ mass distribution is then weighted by the spherical harmonic $Y_L^0(\cos\theta)$ ($L = 1 - 6$). The resulting distributions of the Y_L^0 are shown in Fig. 4. A straightforward interpretation of these distributions is difficult, due to reflections originating from the symmetrization. However, the squares of the spin amplitudes appear in even moments, while interference terms appear in odd moments.

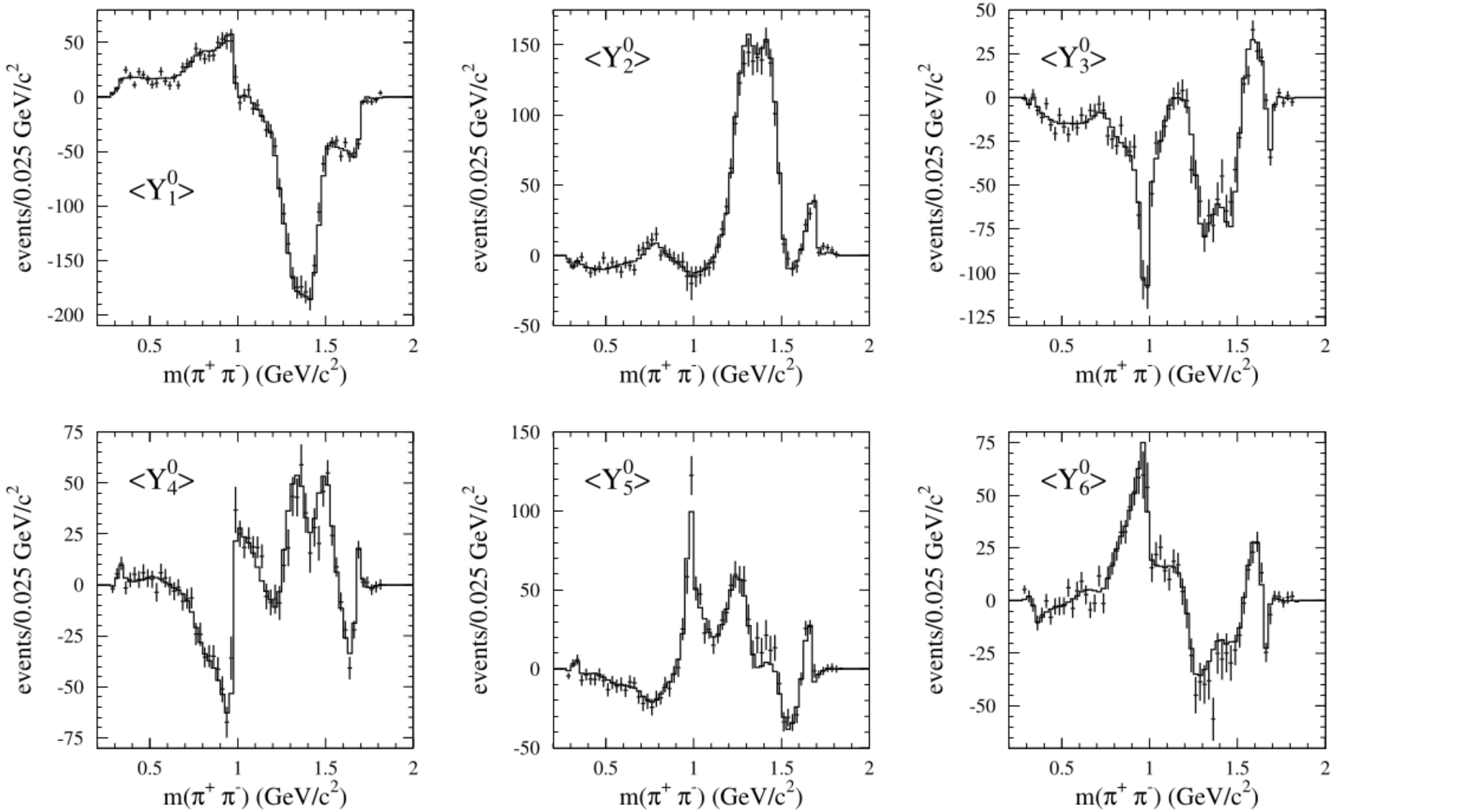

FIG. 4: Unnormalized spherical harmonic moments $\langle Y_L^0 \rangle$ as a function of $\pi^+\pi^-$ effective mass. The data are presented with error bars, the histograms represent the fit projections.

Experimental Results: LASS, 1988

D. Aston *et al*, "A study of K-π+ scattering in the reaction K-p → K-π+n at 11 GeV/c"

Nuclear Physics B, 296(3), 493-526

Abstract

Results from a high statistics study of the reaction $K^-p \rightarrow K^-\pi^+n$ are presented. These results are based on data obtained with an 11 GeV/c beam using the LASS spectrometer at SLAC. The mass dependence of the spherical harmonic moments provides clear evidence for the production of the complete leading orbitally excited K* series up through $J^P = 5^-$. These moments are used to perform an energy independent partial wave analysis of the $K^-\pi^+$ system from threshold to 2.6 GeV/c^2 using a t-dependent parametrization of the production amplitudes. The amplitudes corroborate the leading K*(892), K_2*(1430), K_3*(1780), K_4*(2060), and K_5*(2380) resonances observed directly in the moments, and also provide new evidence for underlying states. The 0^+ amplitude contains the K_0*(1350) and a second 0^+K*(1950) at higher mass. The 1^- K*(1790) seen in earlier two and three-body analyses is confirmed, and evidence is provided for a suppressed $K^-\pi^+$ decay mode of a second 1^- state, the K*(1410), which has been seen in earlier three-body analyses.

Experimental Results: LASS, 1988

D. Aston *et al*, "A study of K-π+ scattering in the reaction K-p→K-π+n at 11 GeV/c"

Nuclear Physics B, 296(3), 493-526

~Partial Waves:

helicity frame. The production angular distribution I_{prod} of the $K^-\pi^+$ system can be expanded as

$$I_{\text{prod}}(m_{K\pi}, t', \Omega) = \frac{1}{\sqrt{4\pi}} \sum_{L,\, M \geqslant 0} t_L^M(m_{K\pi}, t')(2 - \delta_{M0})\mathrm{Re}[Y_{LM}(\Omega)], \quad (3.1)$$

m=0

Experimental Results: LASS, 1988

D. Aston *et al*, "A study of K-π+ scattering in the reaction K-p → K-π+n at 11 GeV/c"

Nuclear Physics B, 296(3), 493-526

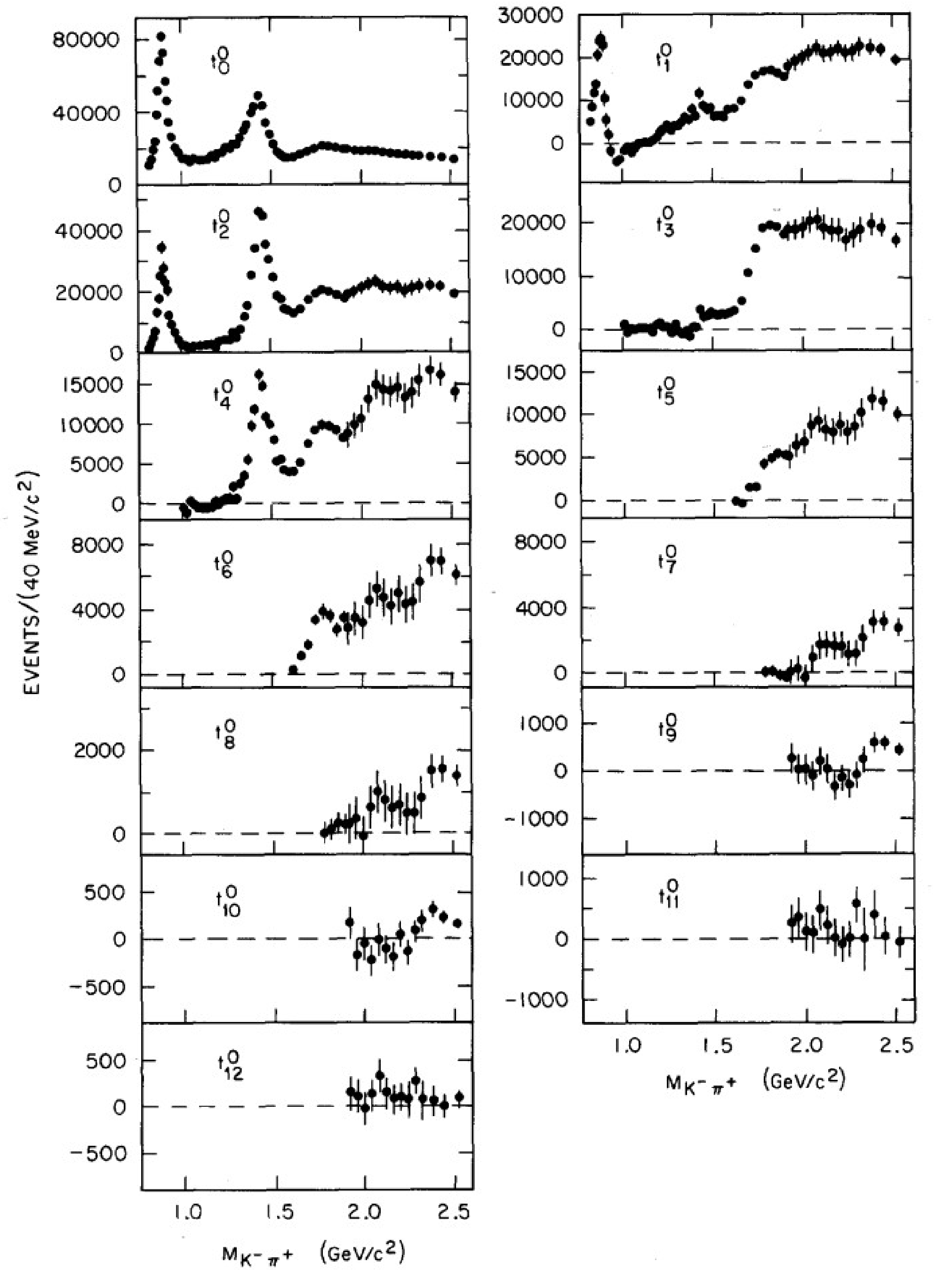

Fig. 6. The acceptance corrected $M=0$ unnormalized $K^-\pi^+$ moments as a function of mass for the small $|t'|$ region, $|t'| \leqslant 0.2\ (\mathrm{GeV}/c)^2$. The notation is defined in eq. (3.1).

m=1

Experimental Results: LASS, 1988
D. Aston *et al*, "A study of K-π+ scattering in the reaction K-p → K-π+n at 11 GeV/c"
Nuclear Physics B, 296(3), 493-526

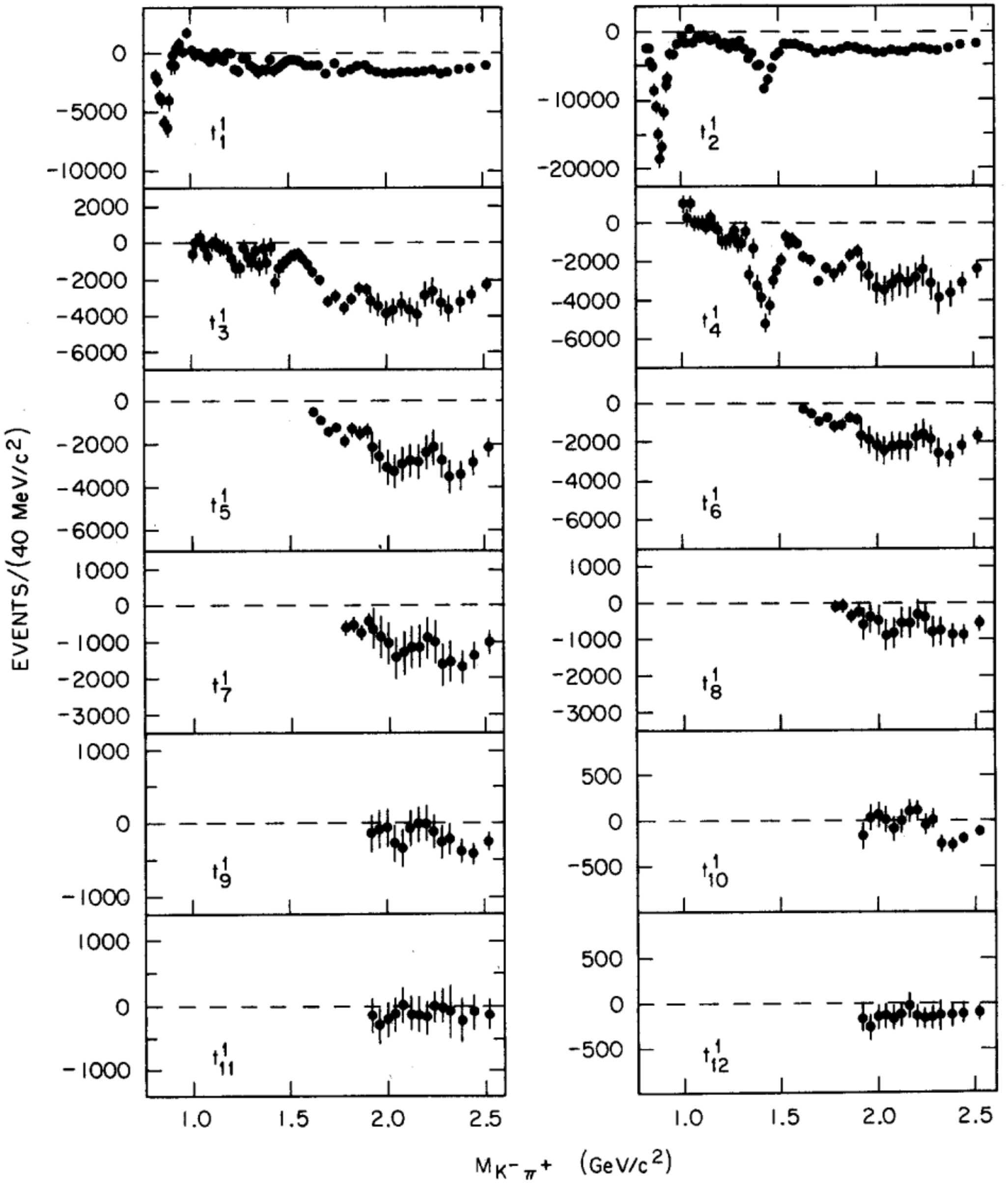

Fig. 7. The acceptance corrected $M=1$ unnormalized $K^-\pi^+$ moments as a function of mass for the small $|t'|$ region, $|t'| \leqslant 0.2\ (\mathrm{GeV}/c)^2$.

PHYSICAL REVIEW D **73**, 032004 (2006)

Model-independent measurement of S-wave $K^-\pi^+$ systems using $D^+ \to K\pi\pi$ decays from Fermilab E791

Analyses typically use an isobar model formulation in which the decays are described by a coherent sum of a nonresonant three-body amplitude NR, usually taken to be constant in magnitude and phase over the entire Dalitz plot, and a number of quasi two-body (resonance + bachelor) amplitudes where the bachelor particle is one of the three final state products, and the resonance decays to the remaining pair. It is assumed that all resonant and NR processes taking part in the decay are described by amplitudes that interfere and have relative phases and magnitudes determined by the decay of the parent meson. In cases where all three decay products are pseudoscalar (P) particles, angular momentum conservation requires that the resonances produced are scalar (S-wave), vector (P-wave), etc . For D mesons, decays beyond D-wave are highly suppressed by the angular momentum barrier factor and can be neglected.

Belle II

University of South Carolina
High Energy Physics Group

PHYSICAL REVIEW D **73**, 032004 (2006)

Model-independent measurement of S-wave $K^-\pi^+$ systems using $D^+ \to K\pi\pi$ decays from Fermilab E791

Analyses typically use an isobar model formulation in which the decays are described by a coherent sum of a nonresonant three-body amplitude NR, usually taken to be constant in magnitude and phase over the entire Dalitz plot, and a number of quasi two-body (resonance + bachelor) amplitudes where the bachelor particle is one of the three final state products, and the resonance decays to the remaining pair. It is assumed that all resonant and NR processes taking part in the decay are described by amplitudes that interfere and have relative phases and magnitudes determined by the decay of the parent meson. In cases where all three decay products are pseudoscalar (P) particles, angular momentum conservation requires that the resonances produced are scalar (S-wave), vector (P-wave), etc . For D mesons, decays beyond D-wave are highly suppressed by the angular momentum barrier factor and can be neglected.

Belle II

University of South Carolina
High Energy Physics Group

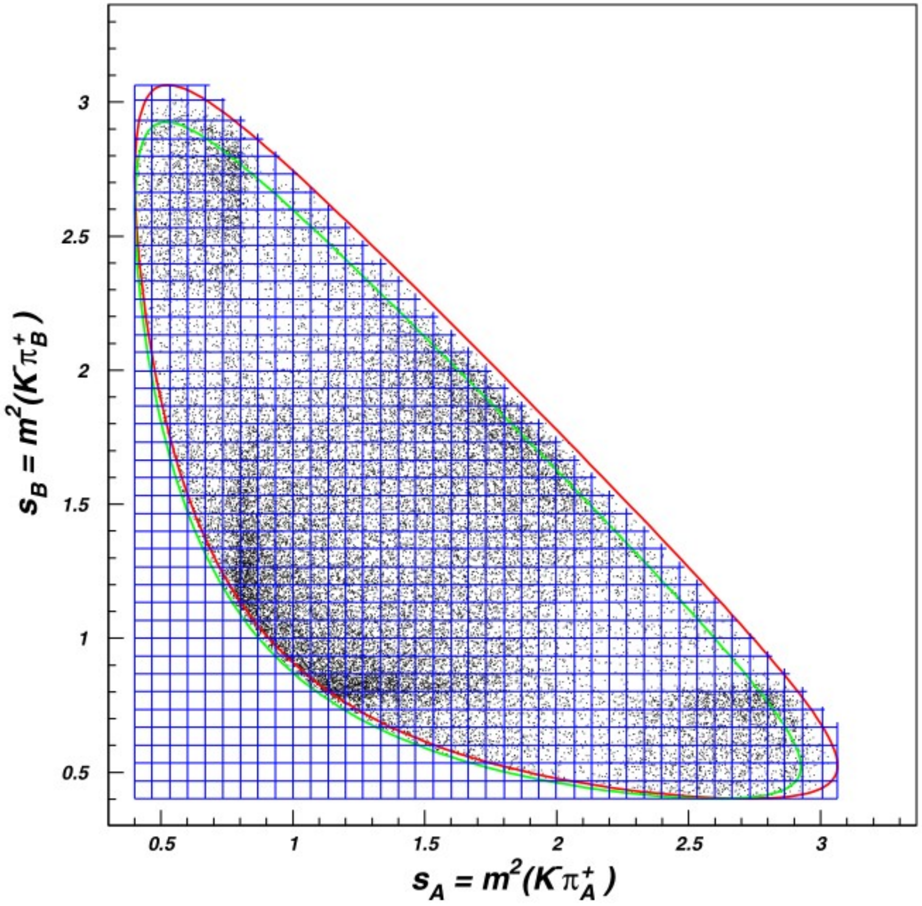

FIG. 1 (color online). Dalitz plot for $D^+ \to K^- \pi_A^+ \pi_B^+$ decays. The squared invariant mass s_B of one $K^-\pi^+$ combination is plotted against s_A, the squared invariant mass of the other combination. The plot is symmetrized, each event appearing twice. Lines in both directions indicate values equally spaced in squared effective mass at each of which the S-wave amplitude is determined by the MIPWA described in Sec. III. Kinematic boundaries for the Dalitz plot are drawn for three-body mass values $M = 1.810$ and $M = 1.890$ GeV$/c^2$, between which data are selected for the fits.

Belle II

USC HEP
University of South Carolina
High Energy Physics Group

E791

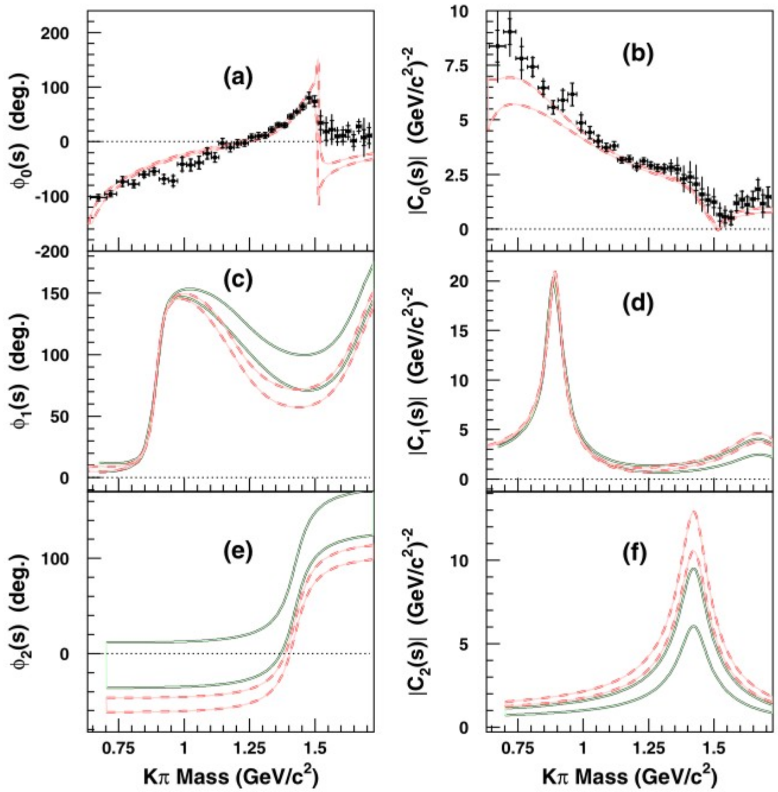

FIG. 3 (color online). (a) Phases $\gamma_k = \phi_0(s_k)$ and (b) magnitudes $c_k = |C_0(s_k)|$ of S-wave amplitudes for $K^-\pi^+$ systems from $D^+ \to K^-\pi^+\pi^+$ decays with the amplitude and phase of the $K^*(892)$ as reference. Solid circles, with error bars, show the values obtained from the MIPWA fit described in the text. The effect of adding systematic uncertainties in quadrature is indicated by extensions on the error bars. The P-wave and D-wave phases are plotted in (c) and (e) and their magnitudes in (d) and (f), respectively. These curves are derived from Eqs. (7) and (8), respectively, evaluated with the parameters and error matrix resulting from the MIPWA. Curves appear as shaded areas bounded by solid line curves representing 1 standard deviation limits for these quantities. In all plots, the dashed curves show 1 standard deviation limits for the predictions of the isobar model fit described in Sec. V. These curves are computed in the same way, using Eq. (17) in addition to (7) and (8) with parameters and error matrix from the isobar model fit.

E791: The Second Solution

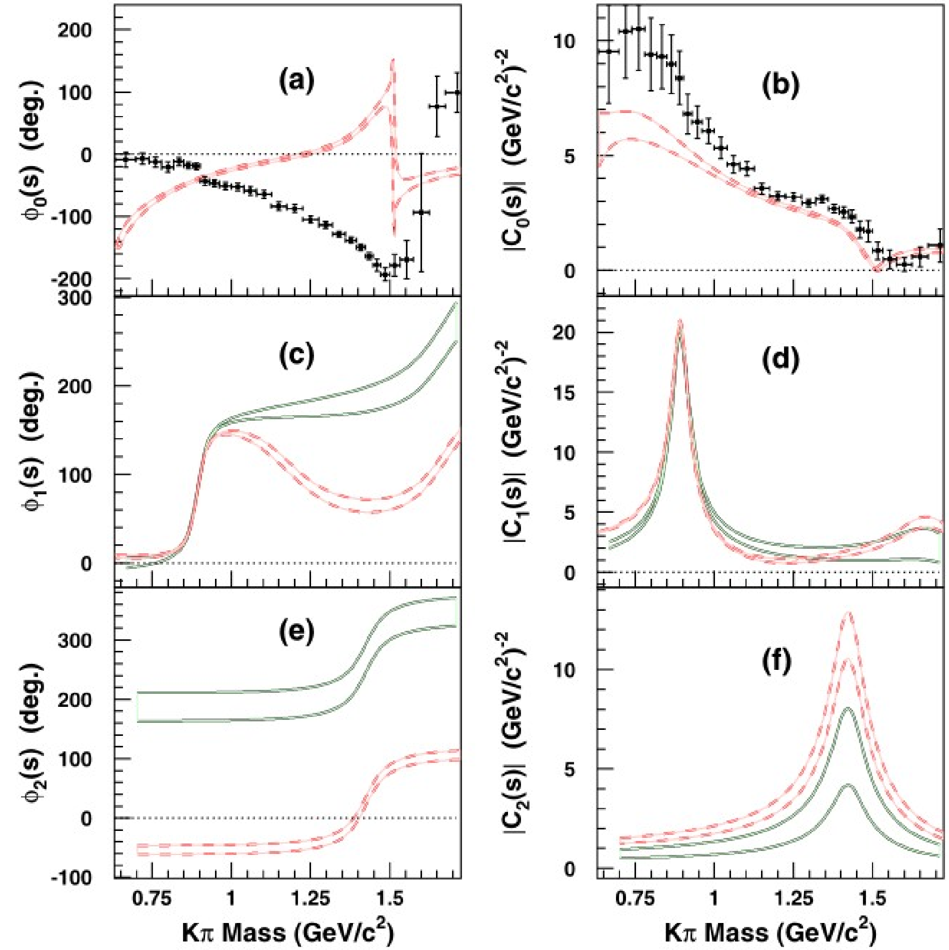

FIG. 9 (color online). A second solution for the S-wave amplitude from MIPWA fits to $D^+ \to K^-\pi^+\pi^+$ decays with P- and D-wave parametrized by the κ model described in the text. Plots show the (a) phase and (b) magnitude for solution B for the S-wave obtained by using different starting values for the amplitudes. The dashed curves delineate the regions that lie within 1 standard deviation of the isobar model fit described in Sec. V. The P-wave is shown in (c) and (d) and the D-wave in (e) and (f).

E791: The Watson Theorem

It is interesting to compare the amplitudes $C_L(s)$ defined in Sec. III and measured in Sec. IV with those from $K^-\pi^+$ scattering, $T_L(s)$. The relationship between C_L and T_L is given by Eq. (6). If the $K^-\pi_A^+$ systems produced in $D^+ \to K^-\pi_A^+\pi_B^+$ decays do not interact with the bachelor π_B^+, then the factor $\mathcal{P}_L(s)$ describes the production of $K^-\pi^+$ as a function of s from these decays. Also, under the same assumptions, the Watson theorem [24] requires that, in the s range where $K^-\pi^+$ scattering is purely elastic, $\mathcal{P}_L(s)$ for each partial wave labeled by L and by isospin I, should carry no s-dependent phase. In other words, ϕ_L, the phase of $C_L(s)$ for each partial wave, should differ, at most, by a constant relative to that of the corresponding elastic scattering amplitude $T_L(s)$. The magnitudes $|C_L(s)|$ and $|T_L(s)|$

E. M. AITALA *et al.*

could differ, however, due to any s-dependence of the production rate of $K^-\pi^+$ systems in D^+ decay.

The validity of the Watson theorem therefore relies on the assumption that no final state scattering between $(K^-\pi_A^+)$ and π_B^+ occurs. This assumption, for decays such as those studied here in which the final state consists of strongly interacting particles, has often been assumed to hold. However, it has never been tested objectively. The MIPWA results from the present data provide, therefore, an interesting opportunity to make such a test and also the opportunity to examine the form for the production factor $\mathcal{P}_L(s)$.

The observed shift in S-wave phase and difference in slope, and the difference in P-wave phase behavior evidenced in Figs. 6(a)–6(c), do not conform to the precise expectations of the Watson theorem.

Conclusions

- There are many complexities in fitting hadronic decays data and many open questions on how best to carry out these fits

- B decays at Belle II have a wider mass range and larger datasets

- Better fits should lead to a better understanding of hadronic
  - Internal structure
  - Spectroscopy
  - Interactions

- Would be nice if we can accurately predict distributions from every hadronic interaction and from every decay!

Extra Slides

Decay angles

$D_s^+ \to \pi^+\pi^-\pi^+$ helicity angle θ, which is defined as the angle between the π^- and the D_s^+ in the $\pi^+\pi^-$ rest frame (or π^+ for D_s^-)